Magued G. Iskander,[1] *Roy E. Olson,*[2] *and James A. Bay*[3]

Design and Performance of an Electro-Pneumatic Pile Hammer for Laboratory Applications

REFERENCE: Iskander, M. G., Olson, R. E., and Bay, J. A., **"Design and Performance of an Electro-Pneumatic Pile Hammer for Laboratory Applications,"** *Geotechnical Testing Journal,* GTJODJ, Vol. 24, No. 1, March 2001, pp. 72–82.

ABSTRACT: Small piles used in research programs have generally been installed by pushing or driving using slow mechanical drop hammers, because of the expense and technical difficulties associated with manufacture of realistic small-scale pile driving hammers. However, pushing does not model inertial effects and slow driving does not model diffusive effects in the soil. It remains to be demonstrated whether these effects are important or not. To help clarify this issue, an electronically controlled, single-acting air hammer, with a rated energy of 211 J (156 ft · lb), and an operating frequency of up to 1.2 Hz, was designed and built. The hammer was used successfully to drive 90 mm (3.5 in.) diameter piles into dense sand under a confining pressure of 138 kPa (20 psi). The behavior of the hammer was documented using detailed measurements of time-dependent ram movements, accelerations, and chamber pressures. This paper is concerned with the design and performance of the hammer.

KEYWORDS: pile hammer, hammer, driving, installation, drivability, pile, piling, deep foundation, calibration chamber, pressure chamber, soil, sand

One of the major obstacles to an improved understanding of the behavior of piles has been the scarcity of full-scale load test data on instrumented piles. Load tests on instrumented full-sized piles may cost millions of dollars (Murff 1992). These high costs have resulted in design procedures that are primarily based on a small number of mostly uninstrumented load tests on full-scale piles, and a few laboratory tests with instrumented piles (Pelletier et al. 1993).

Most laboratory and small-scale field tests have involved burying the "pile" (Vesic 1969), or pushing closed-ended piles into place (Lehane and Jardine 1994). Pushing protects instrumentation and reduces costs significantly, but may not model the behavior of open-ended pipe piles, which plug during static pushing, but remain largely unplugged during driving.

Dynamic and diffusive mechanisms influence pile behavior during and after driving. Dynamic mechanisms involve inertial forces that develop in the pile and soil. Diffusive mechanisms deal with buildup and dissipation of pore water pressure during and after driving. We believe that the installation process is important and, thus, that the design of a small-scale hammer is a prerequisite to proper modeling of the system.

This paper is the first to present the design and performance of a single-acting electro-pneumatic pile hammer, which was developed to install model piles in a laboratory pressure (calibration) chamber. The performance of the hammer was evaluated by monitoring the developed pressures, displacements, forces, and velocities.

Existing Laboratory Hammers

Hammers in One-g Systems

The University of Houston pile hammer was one of the first automatic laboratory pile hammers. It uses a 210 kg (470 lb) ram falling 0.76 m (30 in.) and operates at a rate of 0.33 Hz (Ugaz 1988). It is single acting, air operated, and has an efficiency of 50%.

There are also a number of slow mechanical laboratory drop hammers such as the FHWA hammer. The FHWA hammer, which is used outdoors, has three interchangeable rams ranging between 34 to 227 kg (75 to 500 lb) and has an adjustable stroke of 0.3 to 1.2 m (1 to 4 ft). It operates at 0.08 Hz (Ealy 1999). Slow hammers are capable of modeling dynamic effects during driving but probably cannot model diffusive effects, without changing the viscosity of the pore fluid.

Centrifuge Hammers

Hammers designed for use in centrifuges include those at the universities of Colorado (Mehle 1989), Florida (Gills 1988), Cal. Tech. (Allard 1990), Manchester (Craig 1985), and Cambridge (Nunez 1988). Centrifuge hammers are fast but have tiny rams and strokes. For example, The University of Colorado pile hammer operates at a 25 Hz frequency, but has a ram that weighs 0.17 kg (0.37 lb) and has a stroke of only 12 mm (0.47 in.).

Objectives

The objective of this study was to build a pile hammer that meets the following criteria:

- The hammer must be sufficiently fast so that dynamic and diffusive effects can be studied in fine-grained sand.
- The hammer must be capable of delivering sufficient energy to install piles with static capacities of up to 90 kN (20 000 lb).
- The length of the hammer and its guide system must not exceed one meter (40 in.).
- Noise, pollution, and vibration effects must be limited to a level consistent with indoor operation.

[1] Assistant professor, Department of Civil Engineering, Polytechnic University, 6 Metrotech Center, Brooklyn, NY 11201.
[2] L. P. Gilvin, professor, Department of Civil Engineering, University of Texas, Austin, TX 78712.
[3] Assistant professor, Department of Civil and Environmental Engineering, Utah State University, Logan, UT 84322.

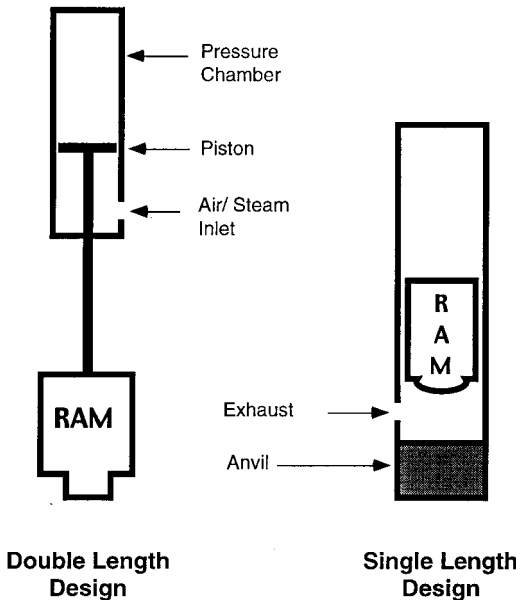

FIG. 1—*Single and double length hammer designs.*

- The hammer must be robust.
- It must be possible to handle the hammer using light hoisting equipment.
- The ram velocity must range between 2 to 3 m/s (7 to 10 ft/s) to satisfy the requirements of impact driving and minimize the likelihood of damage to the pile instrumentation.

Selection of Hammer Type

Initial consideration was given to use of a high-speed electromagnetic hammer (Gills 1988), but such systems cannot handle the needed ram weight, and the high electric fields associated with large electromagnets would make the use of electronic data recording systems difficult. Internal combustion (diesel) hammers were eliminated due to air pollution problems. Double-acting and differential air hammers were considered, but analyses showed that they would be too heavy to be handled conveniently in the laboratory. A single-acting air-operated system was selected. The penalty was the inability to achieve high frequencies, but the advantages included a robust system of reasonable height and weight, and the needed driving energy.

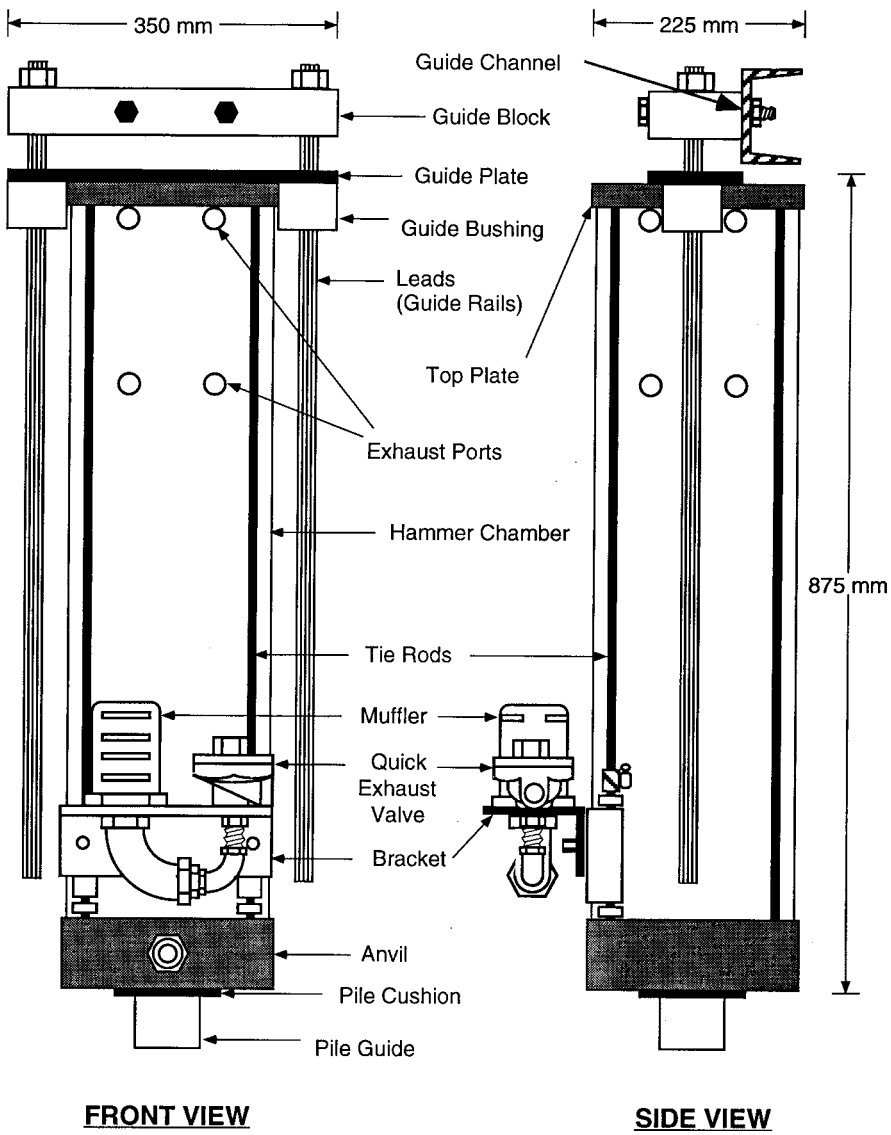

FIG. 2—*Schematic of hammer and leads.*

Most external combustion (steam or air-operated) hammers have a double-length design, while internal combustion (diesel) hammers have a single-length design (Fig. 1). The ram of a double-length hammer is lifted using a piston in an upper chamber. Pressure control valves are located at the base of the pressure chamber. The advantage of a double-length design is that the length of the pressure chamber can be made slightly longer than the stroke of the ram to prevent the piston from impacting the bottom of the chamber and damaging the control valves. In a single-length design, the hammer consists of a single chamber in which the ram is lifted by direct pressure and then dropped to impact an anvil at the bottom of the chamber. The limited laboratory head clearance forced the use of a single-length design and thus required that the control valves be mounted separately from the hammer.

Reduction of cushioning during impact, due to the development of a backpressure ahead of the ram, is achieved in commercial hammers by minimizing the ram's cross-sectional area. The typical length-to-diameter ratio of most production hammers is around 10:1. Limited head clearance in the laboratory required the use of a large-diameter ram in order to maximize the available stroke, thus resulting in a hammer with a 4:1 length-to-diameter ratio.

Airflow in commercial hammers is typically controlled using mechanical trip valves. An electrical control system was chosen for our laboratory hammer because it provides a more versatile control of the hammer's energy and operating frequency.

Layout of the Driving System

The *driving system* consists of three components: the *hammer* (Figs. 2 and 3), a set of *leads* (Figs. 2 and 3), and an external *control unit* which also provides the compressed air (Fig. 4).

FIG. 3—*Photograph of hammer sliding on its leads during driving.*

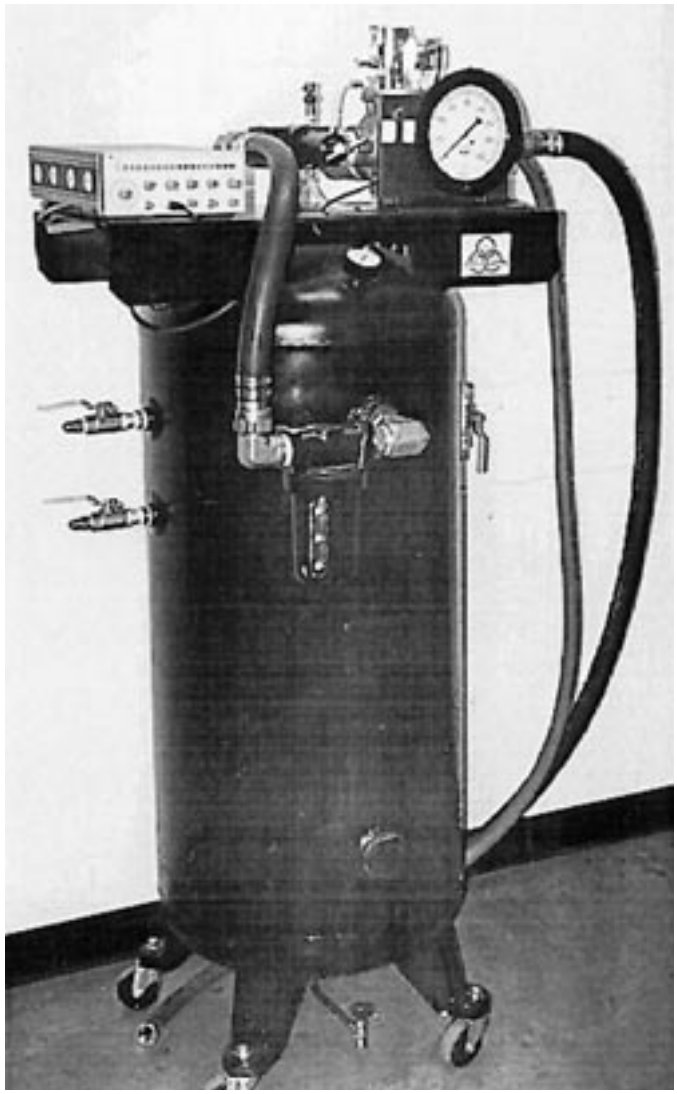

FIG. 4—*Photograph of the control unit.*

The Hammer

The hammer (Fig. 5) consists of a stainless steel ram which slides in an aluminum pressure chamber to impact an anvil at the base of the chamber. The pressure chamber consists of a cylinder, top plate, and the anvil, which are held together using four stainless steel tie rods. The radial clearance between the ram and the cylinder is 0.6 mm (0.025 in.). The ram contains a central ball bushing, which slides on a hardened steel rod, to prevent it from wobbling. The hardened rod is fixed in the top plate and in the anvil.

In an upstroke, air is introduced at the base of the chamber through the air ports in the anvil. The air supply is shut off before the ram reaches its maximum stroke. In a downstroke, the ram falls freely under gravity. During upstrokes, air is exhausted ahead of the ram through six exhaust ports in the top plate and twelve more ports located at two levels in the sides of the cylinder. During downstrokes, air is exhausted ahead of the ram through the pneumatic control system and by blow-by between the ram and the wall of the cylinder.

The Hammer Leads (Guide System)

The hammer leads hold the pile and hammer in proper alignment to prevent eccentric hammer blows. The leads consist of two alu-

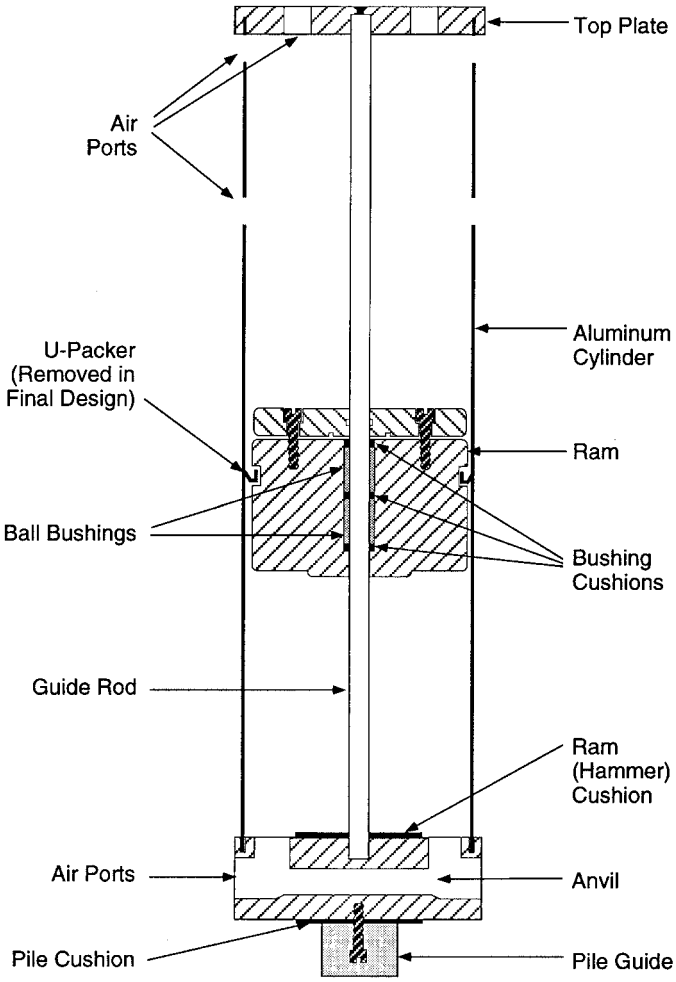

FIG. 5—*Cross section through the hammer.*

minum guide rails connected to a high-density polyethylene (HDPE) guide block (Fig. 2). The block is secured to the pressure chamber's loading frame using an aluminum channel (Fig. 6). As the pile penetrates into the soil, the hammer slides on the guide rails through two low friction HDPE bushings and follows the pile.

The Control Unit

The control unit (Fig. 4) contains the electronic and pneumatic controls. Compressed air used to lift the ram is provided from a solenoid valve, located in the control unit. A function generator controls the solenoid valve and thus controls the operating frequency and stroke of the hammer.

Design of the Hammer

The following is a summary of the hammer design philosophy. Detailed analyses, shop drawings, and component model numbers can be found in Iskander (1995).

Mechanical Design

Wave equation analysis was used to determine the weights, materials, and dimensions of the ram, anvil, and cushions. A separate analysis was performed to study the force-time signal and determine the *dwell time* of contact between the ram and the anvil.

Wave Equation Analyses—Conventional soil properties used in wave equation analyses are generally obtained from back analyses of field case histories. Conditions in a test tank differ from those in the field, so properties obtained from field measurements may not necessarily apply as well in the test tank.

A two-step procedure was used in selecting the proper design parameters. First, wave equation analyses were performed for the driving conditions of the pile tested by Ugaz (1988) at the University of Houston using the computer program WEAP87, and the values of quakes and damping factors that are recommended for full-scale piles (GRL 1987). The capacity measured by Ugaz averaged twice the capacity from wave equation analyses for the same pile set. Next, we assumed that wave equation analyses could be applied for piles in our test tank, using the same wave equation parameters as used above, but with the wave equation capacity equal to half of the anticipated static capacity. Multiple wave equation analyses were then performed to obtain the optimum dimensions and weights of the mechanical components of the pile hammer being designed. These analyses resulted in the selection of the hammer specifications shown in Table 1.

The ram weight is relatively large, compared with the pile weight, because the sand in the test chamber is subjected to a large confining pressure. The usual rule of thumb is that the ram weight should be approximately equal to the weight of the pile being driven (Fleming et al. 1985). However, wave equation analysis of the driving conditions in a test chamber indicates that a ram weighing two to six times the weight of the pile is required.

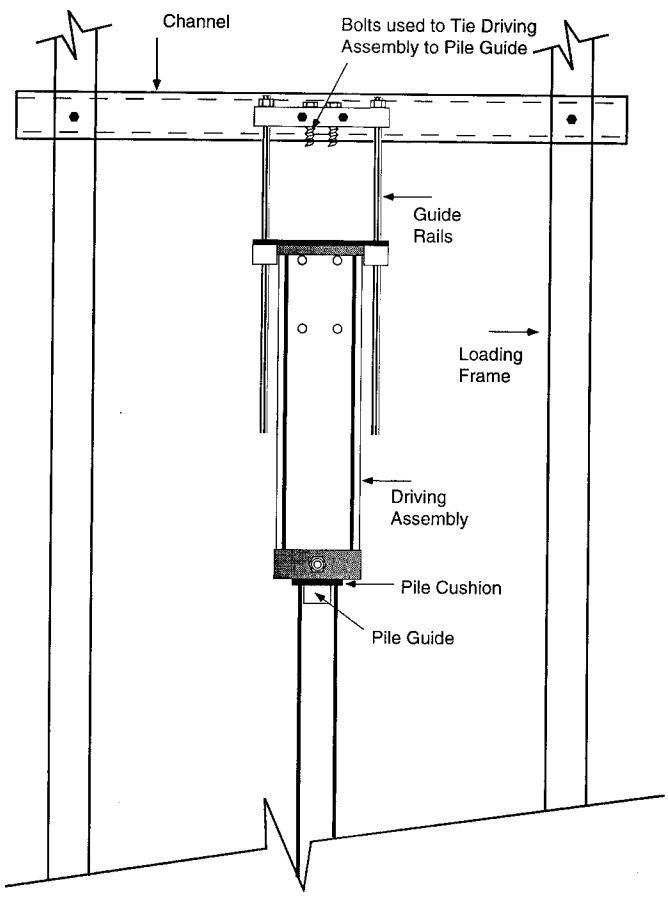

FIG. 6—*Hammer mounted on leads and test frame.*

TABLE 1—*Hammer specifications.*

Item	SI	English
General		
Rated energy	0.21 J	156 ft-lb
Normal operating frequency	1 Hz	60 BPM
Maximum operating frequency	1.2 Hz	72 BPM
Total weight	645 N	145 lb
Efficiency	57–66%	57–66%
Ram (Stainless steel)		
Weight	38 kg	85 lb
Young's Modulus	196 500 MPa	28 500 ksi
OD	208 mm	8.2 in.
ID	20–32 mm	0.8–1.25 in.
Height	152 mm	6 in.
Normal Stroke	560 mm	22 in.
Maximum Stroke	610 mm	24 in.
Anvil (Aluminum)		
Weight	13 kg	30 lb.
Young's modulus	69 000 MPa	10 000 ksi
Dimensions	229 × 229 × 76 mm	9 × 9 × 3 in.
Hammer Cushion (Nylon)		
Young's modulus	2413 MPa	350 ksi
Thickness	1.6 mm	0.0625 in.
Diameter	114 mm	4.5 in.
Pile Cushion (Nylon)		
Young's modulus	2413 MPa	350 ksi
Thickness	1.6 mm	0.0625 in.
OD	102	4.0 in.
ID	63.5 mm	2.5

Dwell Time—In field applications, the main part of the hammer energy is delivered to the pile in a time less than the time of wave propagation to the pile tip and back, t^*. Piles driven in our test chamber have lengths of 0.81 to 0.91 m (32 to 36 in.). For a wave speed, c, of 5000 m/s (16 400 ft/s) in stainless steel, the corresponding wave travel times, t^*, are 0.33 to 0.37 ms. The goal was then to ensure that the time of contact between the ram and anvil (dwell time) is less than 0.33 ms.

The dwell time, t_d, can be approximated as half of the natural period of a system consisting of a mass impacting a spring resting on a rigid base (Warrington 1987):

$$t_d = \pi \sqrt{\frac{m}{k_e}} \tag{1}$$

where m is the mass of the ram and k_e is the equivalent stiffness of the ram cushion, anvil, and pile cushion. Stiffnesses are defined as:

$$k = \frac{E\,A}{L} \tag{2}$$

where E is Young's modulus, A is area, and L is length of the element. The equivalent stiffness, k_e, is given by:

$$k_e = \frac{k_P\,k_R\,k_A}{k_P k_R + k_R k_A + k_P k_A} \tag{3}$$

where k_P is the stiffness of the pile cushion, k_A is the stiffness of the anvil, and k_R is the stiffness of the ram cushion. Using the properties shown in Table 1, the calculated dwell time, t_d, was 0.3 ms, which is shorter than the time for the wave to travel to the tip and return and is thus considered acceptable.

The dwell time calculated using Eqs 1 to 3 neglects the pile stiffness and is only valid for a hammer resting on a rigid system. Deeks and Randolph (1993) developed an alternative analytical model that uses springs and dash pots to represent the pile and cushions and lumped masses to represent the ram and anvil. The model was mathematically unstable for the masses and stiffnesses of our system, which are 2 to 4 orders of magnitude different from those of commercial hammers.

Design of the Electro-Pneumatic Control System

American suppliers of pneumatic components utilize experimentally derived capacity coefficients, c_v, to describe the flow properties of their products (Miller 1984). Capacity coefficients are usually reported in the literature as an index, without units, but actually have units of flow measured in gallons per minute of water at 60°F under a pressure drop of 1 psi (Considine 1957). Equivalent coefficients in metric and SI units were presented by Zappe (1987). We will follow convention in the field and report values of c_v without units. However, the values of c_v must then be calculated using the units specified in the equations, and embedded constants are understood to have units that cause the equations to be dimensionally correct.

In current American industry, gas volumes are specified at a standard temperature of 16°C (60°F) and a standard pressure of 1 atm. Tables from U.S. suppliers use the English system of units. Standard volume is expressed in English units as standard cubic feet (SCF) and flow is standard cubic feet per minute (SCFM). In this paper, standard volume is also reported in standard cubic meters (SCM) and flow in standard cubic meters per second (SCMS).

Required Capacity Coefficient—For computations involving exhausting a pneumatic chamber, like the hammer chamber, capacity coefficients are usually expressed as (Parker 1991):

$$c_v = \frac{a\,S\,A\,C}{T\,29} \tag{4}$$

where

a = area of the chamber (sq. in.),
S = stroke (in.),
A = constant for pressure drop (from manufacturer's tables, e.g., Parker 1991),
C = compression factor (from manufacturer's tables, e.g., Parker 1991), and
T = stroke time (seconds).

To select any component of a pneumatic system, first the required capacity coefficient, c_v, is determined using Eq 4. Next, a component is selected from the pool of commercial components, such that the capacity coefficient of the selected component is larger than that required.

In a downstroke, cushioning of the ram due to the formation of a backpressure is minimized by ensuring that air is capable of exhausting in less time than is needed for the hammer to fall freely under gravitational pull. The time, t, required by the ram to travel the distance, s, from the bottom of the exhaust ports to the anvil, under uniform gravitational acceleration, g, is given by:

$$t = \sqrt{\frac{2s}{g}} \tag{5}$$

For a stroke of 550 mm (22 in.), the travel time of the ram during the downstroke is 0.34 s. A corresponding capacity coefficient, c_v, of 29.6 is obtained by substituting the stroke time, hammer dimensions, and assuming an inlet pressure of 69 kPa (10 psi), and a pressure drop of 14 kPa (2 psi) across the system in Eq 4. Accordingly, all pneumatic components should have a minimum exhaust c_v of 30 to minimize cushioning.

The Electro-Pneumatic Circuit—The hammer is powered by compressed air from a 75 mm (3 in.) diameter main at a peak pressure of about 690 kPa (100 psi). The air is supplied to the control unit through two 12.5 mm (0.5 in.) lines, each with a 0.04 SCMS (80 SCFM) flow capacity (Fig. 7). At the control unit, compressed air is stored in a 0.23 m^3 (60 gal) tank, which functions as a buffer to maintain a constant supply pressure during driving.

At the control unit, compressed air flowing to the hammer passes through a 40 μm filter followed by a high-flow pressure regulator and a solenoid valve. The pressure drop across the filter was about 14 kPa (2 psi) at the range of operating flows.

Flow of air in and out of the hammer chamber is controlled using an externally piloted three-way solenoid valve with an exhaust c_v of 26.9 and a fill c_v of 23.3. The solenoid valve is one of the fastest high-capacity valves commercially available. The solenoid valve is controlled by a solid-state relay, which is controlled by a function generator. Adjusting the frequency and symmetry of the control signal generated by the function generator thus controls the fill and exhaust times of the hammer chamber.

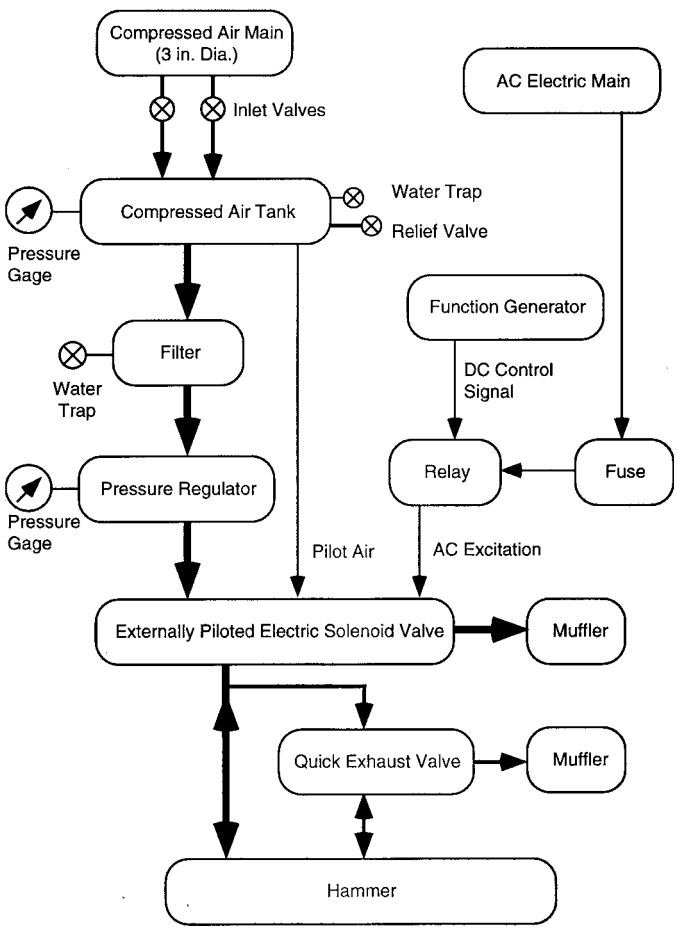

FIG. 7—*Flow chart of the control unit.*

Compressed air that passes through the solenoid valve is divided into two lines going to the hammer chamber. The first line is a 32 mm (1¼ in.) diameter hose, which connects directly to the anvil. A smaller 19 mm (¾ in.) diameter line connects to the anvil through a quick exhaust valve, which is opened to the atmosphere during the downstroke. The quick exhaust is the largest commercially available valve in the United States and has a fill c_v of 8.5, and an exhaust c_v of 11.1 (Ellenger 1993). The quick exhaust valve is considered too small. It is also not possible to synchronize multiple quick exhaust valves in parallel. Accordingly, only one quick exhaust was used to provide secondary exhaust capacity in addition to the main exhaust capacity through the solenoid valve. The total system exhaust capacity is equal to the sum of the capacity coefficients, c_v, of the solenoid and quick exhaust valves and is equal to 38.

Air exhausts to the atmosphere through two mufflers that reduce noise from 115 dB to 92 dB and have a flow capacity of 0.22 SCMS (470 SCFM) each (Ellenger 1993).

Air Consumption—The pressure required to accelerate the ram to the top of its stroke in the required time interval is generally two to five times and pressure needed just to support the ram.[1] About 11 kPa (1.6 psi) is required to support the ram so the required operating pressure is 21 to 55 kPa (3 to 8 psi).

The air consumption of the hammer, in the range of possible operating pressures, is shown in Table 2. The hammer's air consumption per blow (V_c) and maximum air flow (Q_c) are computed from the operating pressure as follows:

$$V_c = A\,S\left(\frac{P_R + P_a}{P_a}\right) \tag{6}$$

$$Q_c = \frac{V_c}{t_e} \tag{7}$$

where

A = cross-sectional area of the cylinder,
S = stroke,
P_R = operating gage pressure,
P_a = atmospheric pressure, and
t_e = time for the ram to travel a distance S.

The preceding estimates depend to a large extent on the amount of blow-by between the ram and its housing, and assume that the ram moves in an upstroke under a uniform acceleration. However, the calculations proved sufficiently accurate for our purposes.

Performance of the Hammer

Two sets of experiments were performed to study the hammer's performance. First, calibration experiments were performed to study the hammer's efficiency, frequency, repeatability, and valve timing under uniform conditions. Next, the performance of the hammer-pile-soil system was studied during driving.

Performance of the Hammer in Calibration Experiments

In the first series of tests, the hammer was placed on a 25 mm (1 in.) thick neoprene pad in order to allow repetitive testing under uniform conditions. Ram movements were monitored using a 760

[1] Personal communication, D. Warrington, Chairman, Vulcan Iron Works, Inc., PO Box 5402, Chattanooga, TN.

TABLE 2—*Air usage of hammer.*

Average Operating Pressure		Air Consumption				Maximum Air Flow	
		Per Blow	Per Minute				
kPa	psi	SCM	SCM	SCMS	SCFM	SCMS	SCFM
35	5	0.025	0.88	0.031	66	0.076	160
69	10	0.031	1.11	0.039	83	0.095	202
103	15	0.038	1.33	0.047	100	0.114	242
138	20	0.044	1.55	0.055	116	0.133	282
172	25	0.050	1.78	0.063	134	0.153	324

mm (30 in.) long LVDT, which was threaded into the ram and extended out of the hammer through an exhaust port in the top plate. The displacements were differentiated with respect to time to obtain the ram velocity. Ram accelerations were measured using an accelerometer mounted on an aluminum rod, which extended out of the hammer through one of the top exhaust ports. A piezoelectric transducer was used to measure the pressures generated in the hammer chamber below the ram.

Hammer Efficiency—The rated energy of a single-acting pile hammer is the maximum theoretical hammer energy. The energy delivered to the anvil is the rated energy times the efficiency, η, where:

$$\eta = \frac{v_i^2}{2gh} \tag{8}$$

where

v_i = ram impact velocity,
g = acceleration due to gravity, and
h = height of fall of the ram.

Initially, we attempted to minimize air consumption by using low friction U-packers to prevent blow-by between the ram and the cylinder (Fig. 5). A preliminary set of experiments with the U-packer in place showed a terminal ram velocity of 1.5 m/s (5 ft/s), a backpressure under the ram of up to 19 kPa (2.8 psi), and an efficiency of 20% at a frequency of 1 Hz.

Next, the packers were removed, thus doubling air consumption. The behavior shown in Fig. 9 was then measured. The impact velocity increased to 2.5 m/s (8.2 ft/s) resulting in an efficiency of 57% at a frequency of 1.2 Hz. The measured efficiency of the laboratory pile hammer compares favorably with the efficiency of production pile hammers which were found to range between 25 to 60% (Chen et al. 1979 and Vines and Amar 1979).

A continuous, electronic signal is sent to the solenoid valve as shown in Fig. 8*a.* A positive signal commands the valve to open and let air into the lower hammer chamber. A negative signal tells the valve to change into the exhaust position. At Point A, the valve is told to open at a time when the ram is still moving downwards from the previous cycle. There is a delay in response, so the valve commands show up at a later time in hammer behavior.

The ram impacts the anvil at Point B (displacement is zero followed by an immediate drop in velocity). At essentially that time, the air has passed through the valve and reached the chamber. The pressure rises suddenly in the small chamber below the ram and reaches a peak at Point C. During that rapid rise in pressure, the

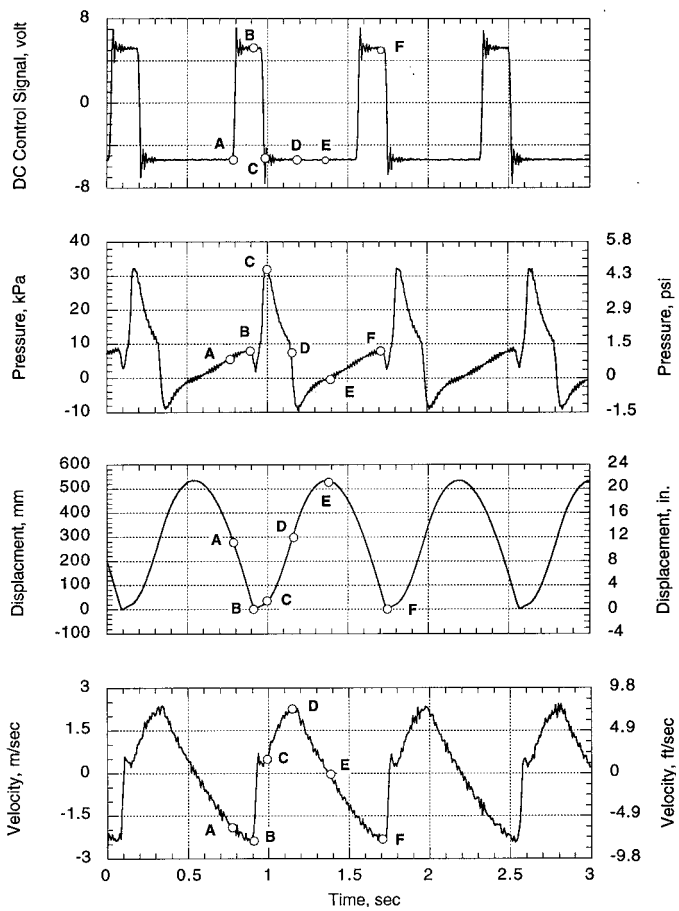

FIG. 8—*Hammer performance during calibration tests:* (a) *control signal,* (b) *chamber pressure below ram,* (c) *ram displacement,* (d) *ram velocity.*

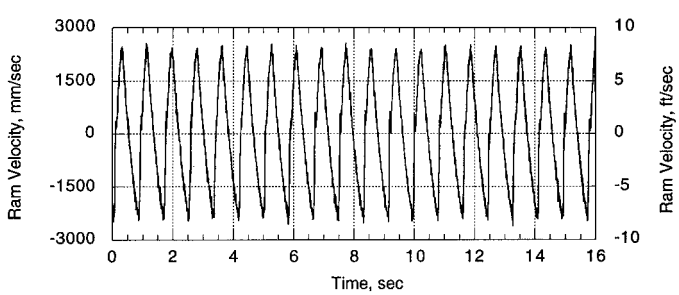

FIG. 9—*Ram impact velocity during 20 successive blows.*

signal is given to shut off the air supply. As the ram accelerates upwards, the pressure drops rapidly. The ram reaches its peak upward velocity at Point D. The ram coasts upwards, now developing a small suction in the lower chamber, and reaches its highest elevation at E. The ram then accelerates downwards to impact the anvil again at Point F.

The energy lost (E_c), due to buildup of backpressure below the ram, was calculated using:

$$E_c = \int_0^{Stroke} paSds \tag{9}$$

where

S = distance traveled by the ram,
p = backpressure, and
a = ram's cross-sectional area.

Integration using Eq 9 and measured values of p indicated that approximately 43% of the potential energy of the ram was lost due to backpressure, so the calculated efficiency of 57% resulted almost entirely from backpressure. Frictional losses are believed to be negligible.

Performance of the Electro-Pneumatic Control System—The function generator, relay, and solenoid valve provided excellent control of the air into the hammer chamber. It was possible to control the air flow such that the ram was energized right after it rebounded from the anvil (Fig. 8, Point B). The airflow was terminated before the hammer reached full stroke (Fig. 8, Point C), thereby reducing the air consumption and the volume of exhaust air.

For the downstroke, the backpressures were larger than calculated, based on flow coefficients provided by the manufacturer. The flow coefficients may be lower during intermittent use in the hammer than for continuous flow as used by the manufacturers for their design tables.

Repeatability—Data from multiple blows were recorded to check the hammer's repeatability. In one typical set of 20 blows with the hammer on the neoprene cushion (Fig. 9), the mean impact velocity was 2.50 m/s (8.2 ft/s) with a coefficient of variation of only 2%. Larger variations in behavior occurred during actual pile driving because the response of the pile changed during driving.

Accelerations and Velocities—Measured peak ram accelerations at impact were approximately 2000 g. Integration of the acceleration trace led to a calculated ram velocity at impact of 2.6 m/s (8.5 ft/s).

Hammer Performance During Pile Driving

The hammer was used to drive a closed-ended steel pipe pile into dense dry sand in a test chamber under a 138 kPa (20 psi) confining pressure. The pile was 0.9 m (3.5 in.) in outer diameter, 0.84 m (33 in.) long, and had a 3 mm (0.12 in.) wall thickness. The pile was provided with an accelerometer, an LVDT, and strain gages, mounted on its side near its top. The accelerations were integrated to obtain pile head velocities (V) and then converted to equivalent forces (F) using (Goble et al. 1980):

$$F = \sigma A = \frac{EA}{c} V \tag{10}$$

where A and E are the pile's cross-sectional area and Young's modulus, respectively; c is the wave speed taken as 5000 m/s (16 400 ft/s); and σ is the stress. Forces and velocities can thus be plotted to the same scale.

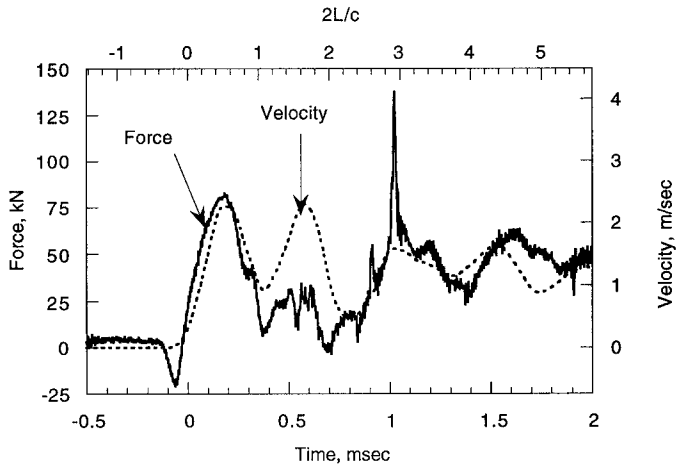

FIG. 10—*Pile head force and velocity measurements during driving (average 200 blows).*

Force-Time Curve—The goal was to have a driving system that would generate enough force to penetrate the piles in a reasonable number of blows. The measured pile head forces (from strain gages on the pile) and velocities (integrated accelerations converted to equivalent forces using Eq 10) are compared in Fig. 10, where the data are the average of 200 blows.[2]

The return time of the stress wave from the pile tip ($2L/c$) should have been about 0.35 ms. The sudden separation of the velocity and force traces at a time of about 0.35 ms indicates that a tension wave was reflected from the pile tip. When the reflected tension wave reached the pile top, the heavy ram provided relative fixity so the tension wave was reflected from the top as a tension wave. The tension wave cancels much of the compression from the incident wave (force trace drops) and increases the downwards velocity (velocity trace rises). The resulting tension wave reflects off the tip as a compression wave and reaches the pile top where it is reflected as a compression wave. The reflected compression wave combines with the incident compression wave, resulting in a large increase in the compression force and a corresponding increase in the downwards velocity.

Hammer Efficiency During Driving—The energy transferred into a rod in an axial impact, E_i, is given by Timoshenko and Goodier (1970):

$$E_i = \int_0^{\infty} F(t)v(t)dt \tag{11}$$

Where $F(t)$ and $v(t)$ are the force and velocity, measured at a point near the edge of the rod. Butler et al. (1998) and Farrar (1998) applied this technique to calculate the efficiency of SPT hammers. A variation of the same method has also been employed in ASTM Standard Test Method for Stress Wave Energy Measurement for Dynamic Penetrometer Testing Systems, D 4633-86. The integrated energy input to the pile is calculated in Fig. 11 and found to be 140 J (103 kip-ft). This energy corresponds to a hammer efficiency of 66%.

[2] A closed-ended pile was used such that the pile reached refusal and little movement occurred per blow.

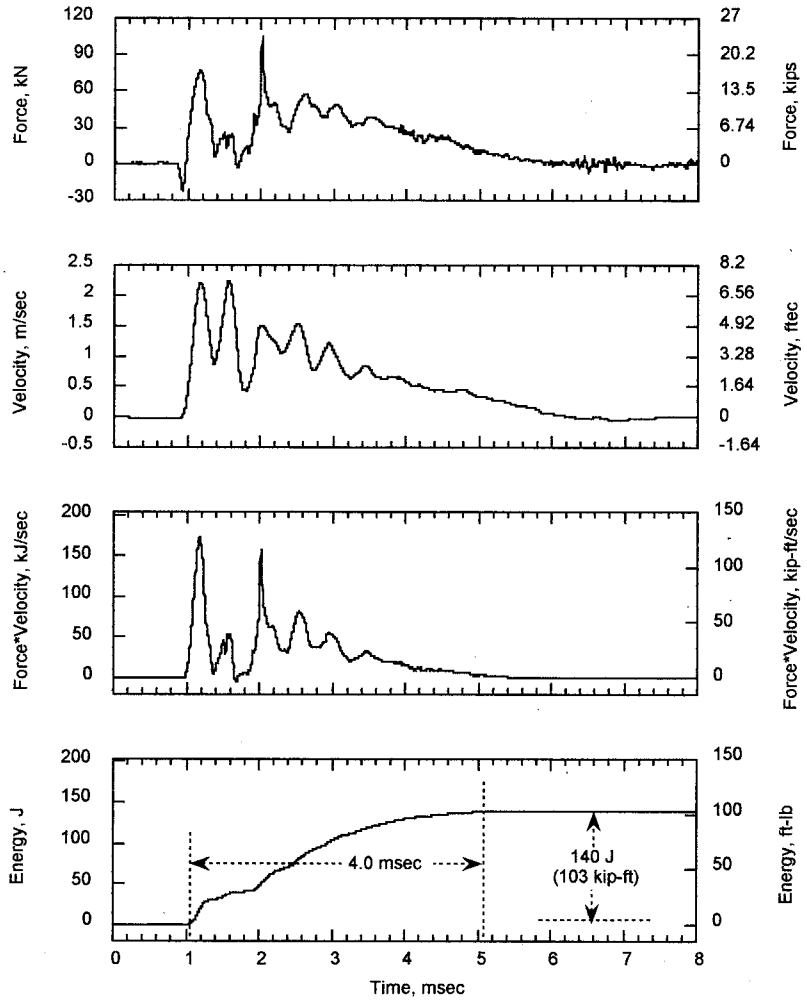

FIG. 11—*Energy delivered to the pile:* (a) *measured force,* (b) *velocity (integrated from acceleration),* (c) *force* velocity, and* (d) *energy (integrated from* (c)*).*

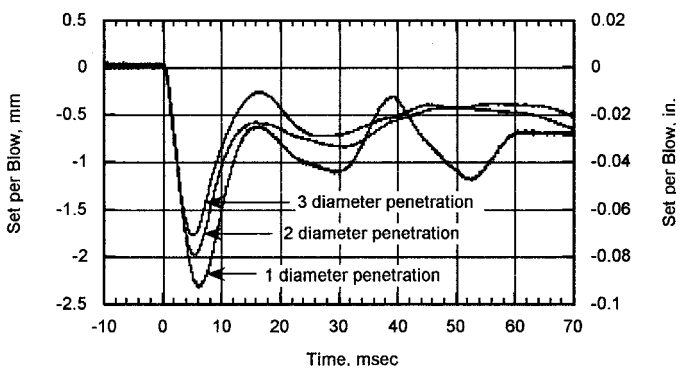

FIG. 12—*Measured tip penetration at various depths in the sand.*

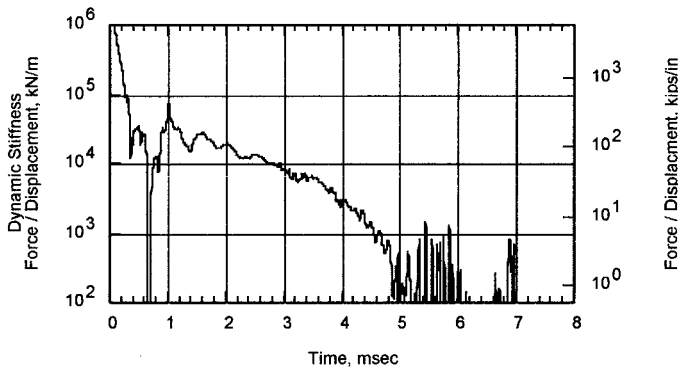

FIG. 13—*Dynamic pile-soil stiffness during impact.*

Pile Set—Measured peak settlements generally exceeded 1.25 mm (0.05 in.) per blow, whereas the final net settlement (the "set") was of the order of 0.5 mm (0.02 in.) per blow (Fig. 12). These are essentially the values assumed in the design of the hammer. The elastic deformation in Fig. 12 exceeds the elastic compression of the pile by several orders of magnitude and is primarily caused by the elastic deformation of the soil in end bearing.

Ram Dwell Time—The measured dwell time, in Fig. 11*d,* was approximately 4 ms, which is one order of magnitude larger than that calculated using Eqs 1 to 3 for the ram impacting the anvil. The system response was dominated by the soft response of the soil-pile system. The dynamic stiffness of the soil-pile system varies within three orders of magnitude during impact (Fig. 13). An approximate dynamic stiffness, K_d, can be calcu-

lated as follows:

$$K_d = \frac{F_{\max}(t)}{S_{\max}(t)} = \frac{80 \text{ kN (18 kips)}}{2 \text{ mm (0.08 in.)}} = 40 \text{ } MN/m \text{ (225 kips/in.)} \quad (12)$$

where $F_{\max}(t)$ is the maximum pile head force measured in Fig. 10, and $S_{\max}(t)$ is the average maximum pile head deformation per blow (not final set) measured in Fig. 12. The equivalent stiffness of the hammer/cushions is two orders of magnitude larger than that of the pile/soil system, and can thus be neglected when calculating the soil/pile/cushions/hammer stiffness.

A dwell time of 4.0 ms can be calculated by substituting the mass of the hammer, *not the ram,* (645 N, 145 lb) and the dynamic stiffness of the soil/pile/cushions/hammer system in Eq 1. Therefore, it is evident that when the ram impacts the anvil, they move in phase while applying their combined weight to the pile. The length of the dwell time depends totally on the stiffness of the soil-pile system.

Wave Equation Analyses—As expected in the preliminary analysis, WEAP underestimated capacity by about 40%. Piles were driven to a resistance of about 1970 bpm (600 bpf) and the corresponding wave equation capacity was approximately 45 kN (10 kips). Static loading tests yielded a capacity of about 63 kN (14 kips).

The properties used in the initial analyses did not lead to a good match between measured and calculated stresses and pile head velocities. The pile driving process led to shock waves that emanated out to reflect off the sides of the metal pressure chamber. The assumption of a pile in a half space was invalidated at an early stage and consideration was concentrated on the first $2L/c$ time period (about 0.4 ms). The best fit was achieved using side and tip quakes of 0.02 in. (the same as the set), side and tip damping factors of 0.4 s/ft, and reducing the cushions' stiffness by half.

Conclusions

An electro-pneumatic pile driving hammer was developed for laboratory use. It was successful in driving 90 mm (3.5 in.) diameter piles with capacities reaching up to 68 kN (15 kips) into dense sands. The hammer performance was validated using detailed measurements. The hammer delivered a repeatable rated energy of 211 J (156 ft · lb) with a 66% efficiency. The maximum impact velocity and operating frequency are 2.5 m/s (8.2 ft/s) and 1.2 Hz, respectively. The electro-pneumatic components provided excellent control of the hammer frequency, velocity, stroke, and energy. The dwell time was dominated by the low stiffness of the soil, and could not be controlled.

Acknowledgments

The work presented herein was supported in part by the Offshore Technology Research Center (NSF Engineering Research Centers Program, Grant No. CDR8721512). The authors wish to thank the Offshore Technology Research Center for its financial support.

References

Allard, M., 1990, "Soil Stress Field Around Driven Piles," Dissertation, California Institute of Technology.

Butler, J., Caliendo, J., and Goble, G., 1998, "Comparison of SPT Energy Measurement Methods," *Proceedings, Geotechnical Site Characterization,* P. Robertson and P. Mayne, Eds., Balkema, pp. 901–905.

Chen, D., Toto, J., and Wong, I., 1979, "Field Evaluation of Hammer Efficiency and Pile Driving Criteria," *Proceedings ASCE Piling Symposium,* F. M. Fuller, Ed., Atlanta, GA.

Craig, W., 1985, "Modeling of Pile Installation in Centrifuge Experiments," *Proceedings Eleventh ICSMFE,* Vol. 2, pp. 1101–1104.

Considine, D., 1957, *Process Instruments and Controls Handbook,* McGraw-Hill Book Company, New York.

Deeks, A. and Randolph, M., 1993, "Analytical Modeling of Hammer Impact for Pile Driving," *International Journal of Numerical and Analytical Methods in Geomechanics,* Vol. 17, pp. 279–302.

Ealy, C., 1999, *Personal Communications, FHWA,* 6300 Georgetown Pike, McLean, VA.

Ellenger, W., 1993, Proprietary Test Data, Parker Hanafin Corporation, Richland, MI.

Farrar, J., 1998, "Summary of Standard Penetration Test Energy Measurements Experience," *Proceedings, Geotechnical Site Characterization,* P. Robertson and P. Mayne, Eds., Balkema, pp. 919–926.

Fleming, W., Weltman, A., Randolph, M., and Elson, W., 1985, *Piling Engineering,* John Wiley and Sons, NY.

Gills, J., 1988, "Development and Testing of a Device Capable of Placing Model Piles by Driving and Pushing in the Centrifuge," dissertation, University of Florida.

Goble, G., Rausche, F., and Likins, G., 1980, "The Analysis of Pile Driving, A State of the Art," *International Seminar on the Application of Stress Wave Theory on Piles,* Stockholm, Balkema, pp. 131–161.

GRL, 1987, "Wave Equation Analysis of Pile Foundations," *WEAP86 Program, 1987 Issue,* Vols. 1–4, Federal Highway Administration, McLean, VA.

Hirsch, T., Carr, L., and Lowery, L., Jr., 1976, "Pile Driving Analysis," *Wave Equation Users Manual TTI Program,* Vols. 1–4, FHWA-IP-76-13.

Iskander, M., 1995, "An Experimental Facility to Model the Behavior of Piles in Sand," *Ph.D. Dissertation,* University of Texas, Austin, TX.

Lehane, B. and Jardine, R., 1994, "Shaft Capacity of Driven Piles in Sand: A New Design Approach," *Proceedings, Seventh International Conference on the Behaviour of Offshore Structures,* Vol. 1, Pergamon Press, pp. 23–36.

Mehle, J., 1989, "Centrifuge Modeling of Pile Driving," Master Thesis, Department of Civil, Environmental, and Architectural Engineering, University of Colorado, Boulder, CO.

Miller, D., 1984, "Compressible Internal Flow," British Hydromechanics Research Association (BHRA), Fluid Engineering Series, BHRA, Vol. 10.

Murff, J. D., 1992, personal communication, Exxon Production Research Company, Houston, TX.

Nunez, I., Hoadley, P., Randolph, M., and Hulett, J., 1988, "Driving and Tension Loading of Piles in Sand on a Centrifuge," *Proceedings, Centrifuge 88,* Balkema, pp. 353–362.

Parker, 1991, "Parker Pneumatic Products Catalog 0107-1," Pneumatic Division, Parker Hanafin Corporation, Richland, MI.

Pelletier, J., Murff, J. D., and Young, A., 1993 "Historical Development and Assessment of the Current API Design Methods for Axially-Loaded Pipes," *Proceedings, Offshore Technology Conference,* Houston, TX, OTC Paper No. 7157, pp. 253–282.

Timoshenko, S. and Goodier, J., 1970, *Theory of Elasticity,* McGraw Hill, New York.

Ugaz, O., 1988, "An Experimental and Numerical Study of Impact Driving of Open-Ended Pipe Piles in Dense Saturated Sand," Dissertation, University of Houston.

Vesic, A. S., 1969, "Experiments with Instrumented Pile Groups in Sand," *Performance of Deep Foundations, ASTM STP 444,* pp. 177–222.

Vines, W. and Amar, J., 1979 "Stress Measurements for Offshore Pile Driving," *Proceedings, ASCE Piling Symposium,* Frank M. Fuller, Ed., Atlanta, GA.

Warrington, D., 1987, "A Proposal for a Simplified Model for the Determination of Dynamic Loads and Stresses During Pile Driving," *Proceedings, 19th Offshore Technology Conference,* Houston, TX OTC paper No. 5395.

Zappe, R. W., 1987, *Valve Selection Handbook,* 2nd ed., Gulf Publishing Company, P.O. Box 2608, Houston, TX.